NANO LETTERS

Letter

pubs.acs.org/NanoLett

Adsorbate-Induced Curvature and Stiffening of Graphene

Simon A. Svatek,[†] Oliver R. Scott,[†] Jasmine P.H. Rivett,[†] Katherine Wright,[†] Matteo Baldoni,[‡] Elena Bichoutskaia,[‡] Takashi Taniguchi,[§] Kenji Watanabe,[§] Alexander J. Marsden,[∥] Neil R. Wilson,[∥] and Peter H. Beton*[,†]

[†]School of Physics and Astronomy, University of Nottingham, Nottingham NG7 2RD, United Kingdom

[‡]School of Chemistry, University of Nottingham, Nottingham NG7 2RD, United Kingdom

[§]The National Institute for Materials Science, Advanced Materials Laboratory, 1-1 Namiki, Tsukuba, Ibaraki 305-0044, Japan

[∥]Department of Physics, University of Warwick, Coventry CV4 7AL, United Kingdom

Supporting Information

ABSTRACT: The adsorption of the alkane tetratetracontane (TTC, $C_{44}H_{90}$) on graphene induces the formation of a curved surface stabilized by a gain in adsorption energy. This effect arises from a curvature-dependent variation of a moiré pattern due to the mismatch of the carbon−carbon separation in the adsorbed molecule and the period of graphene. The effect is observed when graphene is transferred onto a deformable substrate, which in our case is the interface between water layers adsorbed on mica and an organic solvent, but is not observed on more rigid substrates such as boron nitride. Our results show that molecular adsorption can be influenced by substrate curvature, provide an example of two-dimensional molecular self-assembly on a soft, responsive interface, and demonstrate that the mechanical properties of graphene may be modified by molecular adsorption, which is of relevance to nanomechanical systems, electronics, and membrane technology.

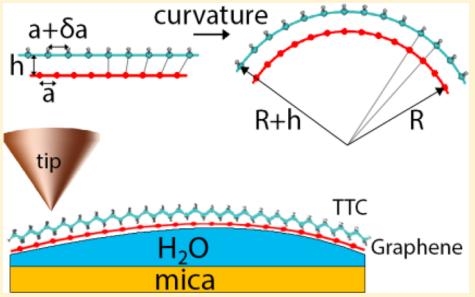

KEYWORDS: *graphene, water, mica, STM, alkanes*

Two-dimensional supramolecular assembly of organic molecules on graphene is currently attracting great interest because it provides a method to control the spatial organization of adsorbates that are known to modify the chemical and electronic properties of graphene.[1,2] Studies of supramolecular organization have, so far, focused on graphene which adheres strongly to rigid supporting substrates such as SiC,[3,4] metal surfaces,[5−7] or most relevant to potential applications,[8−10] dielectrics. These investigations have provided interesting insights that may be understood within well-established models of molecular adsorption, whereby the graphene is treated as a passive, quasirigid layer. However, one of the many interesting properties of graphene is its intrinsic flexibility,[11] and here, we describe an example in which the graphene actively responds, through mechanical deformation, to the adsorption of molecules. Specifically, we observe that the supramolecular organization of adsorbed alkane chains induces curvature and anisotropic mechanical properties in a graphene monolayer, which, in our experiments is suspended between trapped water layers and an organic solvent. Our results show that molecular adsorption can influence the mechanical properties of graphene and, thus, is relevant to applications in electronic materials, membrane technologies, and micromechanical systems. In addition, we extend current studies of surface supramolecular organization to encompass adsorption on soft, deformable interfaces that must be treated as responsive, rather than passive, surfaces.

The substrates for our experiments are prepared by transferring monolayer graphene grown by chemical vapor deposition onto dielectric substrates[12] (full details are provided in Supporting Information). Following further cleaning steps, a solution of the *n*-alkane tetratetracontane (TTC; $C_{44}H_{90}$) in tetradecane ($C_{14}H_{30}$) is drop-deposited on the surface. Images of TTC molecules absorbed at the graphene/solvent interface are acquired using a scanning tunneling microscope (STM) operating in constant current mode under ambient conditions using a cut PtIr wire as an STM tip. Full details of all experimental procedures are provided in the Supporting Information.

We have investigated the adsorption of TTC on graphene (G) transferred to either exfoliated hexagonal boron nitride (hBN) flakes on a supporting SiO_2 layer[13] or onto mica.[14] STM images of TTC on G/hBN and G/mica (Figure 1) show lamellar rows of molecules that run continuously over graphene both on the relatively smooth hBN and also on the rougher G/mica substrate. The lamellar arrangement is most clearly resolved for TTC on G/hBN (Figure 1a−c) and is very similar to the arrangement for analogue alkanes[15−17] adsorbed on graphite. The rows in Figure 1a are superposed on a hexagonal moiré pattern arising from the orientational mismatch between

Received: August 28, 2014
Revised: November 10, 2014

   dx.doi.org/10.1021/nl503308c | *Nano Lett.* XXXX, XXX, XXX−XXX

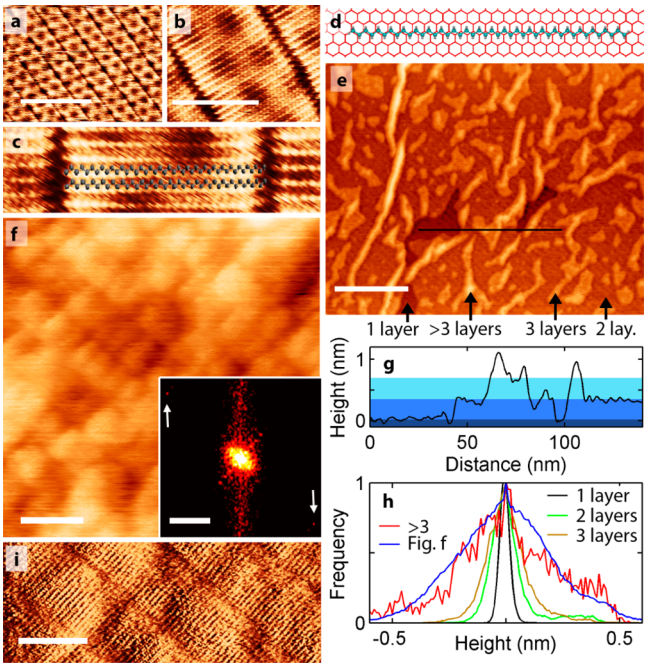

Figure 1. (a–c) TTC on G/hBN. (a) Lamellar rows of TTC on G/BN; the G/BN moiré pattern is also resolved. Scale bar: 20 nm (sample voltage −1 V, tunnel current 0.07 nA). (b) High resolution STM image of lamellar rows. Scale bar: 5 nm (−1 V, 0.1 nA). (c) Zoom of (b) showing atomic resolution. (d) Schematic of adsorption of an *n*-alkane on graphene. Due to the mismatch in lattice constants, $-CH_2-$ groups are adsorbed at different local environments on the flat graphene. (e) TTC on G/mica. The lamellar structure runs continuously across several 100 nm and over terrace edges introduced by water layers. Scale bar: 60 nm (−1 V, 0.15 nA). (f) TTC on G/mica. Strong anisotropy of the shape of trapped water is apparent in areas where more than three layers of water are trapped. Scale bar: 10 nm (−1 V, 0.15 nA). Inset: Fourier transform of image showing an elliptical central spot indicating deformation of underlying graphene; the molecular structure along the lamellae gives rise to the spots identified by arrows; inverse length scale bar 1 nm^{-1}. (g) Profile along marked line in (e) showing step heights across water layer. (h) Histogram of heights for different number of water layers trapped at the G/mica interface indicating an increasing roughness for a higher number of trapped water layers. (i) Differential image of TTC on G/mica with >3 layers of water showing that the expected molecular arrangement within the lamellar rows; the undifferentiated image is included in Supporting Information. Scale bar: 6 nm (−1 V, 0.15 nA).

the transferred graphene and the hBN supporting substrate.[18−20] The presence of the moiré pattern confirms that the G and hBN are in direct contact, indicating that the adhesion between these surfaces is maintained in the presence of the TTC/tetradecane solution.

Further STM images (Figure 1b and c) show the molecular arrangement within the lamellar rows and provide intramolecular resolution showing the zigzag structure of the alkane. The separation of the lamellar rows is 5.8 ± 0.1 nm and the separation of molecules within the row is 0.42 ± 0.01 nm, in agreement with the expected[15−17] value, $\sqrt{3}a$, where a is the graphene lattice constant. Figure 1d is a schematic showing the adsorption of alkanes on graphite.[15−17] There is a mismatch between the graphite lattice constant and the separation of alternate carbon atoms in the alkane, $a_{alk} = a + \delta a$. A consequence of this mismatch is that not all carbon atoms in the alkane can be simultaneously adsorbed above their preferential adsorption sites (see Figure 1d).[15−17]

Figure 1e and f shows STM images of the G/mica surface following the deposition of TTC. A large area image (Figure 1e) shows a terrace-like morphology arising from graphene overlaid on regions where there are varying numbers of trapped water layers at the G/mica interface.[21−25] In previous studies, it has been reported that trapped water forms, predominantly, ice-like monolayer or bilayer islands,[21,23,24] and that graphene transfer methodologies involving the immersion of mica in water[22] result in the adsorption and trapping of at least one layer, and in most areas two or more layers, of water. It was also found that terrace steps could no longer be resolved if more than three layers of water were trapped. In such regions, the roughness of graphene increases significantly, and this was attributed to a liquid-like thicker film of trapped water.[21,22] The adsorption of molecules on such regions forms the focus of this work.

Following He et. al.,[22] we identify the lowest contrast level in Figure 1e as a single trapped water layer. The step heights between the plateaus 1−2 and 2−3 marked in Figure 1e are extracted from line profiles (Figure 1g) and are 0.36 ± 0.03 nm and 0.42 ± 0.03 nm, respectively, in good agreement with reported values which range from 0.35 nm to 0. 42 nm.[21−24] In common with previous work, the roughness increases as the number of trapped water layers increases. Figure 1h shows a histogram of heights and we find a roughness value of 0.05 nm (taken as the full width half-maximum) for a single water layer, which increases to 0.10 nm (0.12 nm) for two (three) water layers. A big increase in roughness to ∼0.40 nm occurs where the number of trapped layers is greater than three. This roughness value is comparable with the layer height, indicating, as suggested in previous studies,[21,22] that the water is not ice-like at these thicknesses.

The TTC lamellar structure runs continuously across step edges introduced by the layered nature of the trapped water and may be resolved in Figure 1e as diagonal lines separated by 5.8 nm, which have an unbroken length of ∼250 nm across the entire image. Differential images showing the extended lamellae and the intersection of the rows with water-induced terrace steps are included in the Supporting Information; our data shows that the supramolecular arrangement is maintained as the rows run over terrace steps of height ∼0.3−0.4 nm.

Figure 1f shows an STM image of TTC adsorbed on an area with >3 layers of water. The lamellar structure is visible, but in addition, the roughness—apparent in the background contrast variation—is anisotropic; many of the brighter regions have an elliptical shape with the long axis aligned in a fixed orientation which is perpendicular to the lamellar rows. The molecular structure within the lamellar rows may also be resolved; see Figure 1i and additional images in the Supporting Information. The anisotropy is also clear in the two-dimensional fast Fourier transform (FFT) of the STM image (Figure 1f inset), which shows a series of spots arising from the periodic lamellar rows (a diffraction spot due to the packing along the rows is also resolved at higher wavevector and is marked by arrows) superimposed on an elliptical central spot. This ellipticity confirms the anisotropic nature of the background fluctuations of the surface. In particular, nonperiodic fluctuations with characteristic length scales, which are smaller than the molecular length, are present parallel to the lamellar rows but strongly suppressed in the perpendicular direction. Importantly, this anisotropy indicates that the supramolecular structure is not simply a periodic arrangement overlaid on a passive surface but a structure which modifies the underlying graphene.

dx.doi.org/10.1021/nl503308c | *Nano Lett.* XXXX, XXX, XXX−XXX

A comparison of the variation of heights across the lamellar rows for TTC adsorbed on different substrates is shown in Figure 2. When adsorbed on G/hBN the height variation is

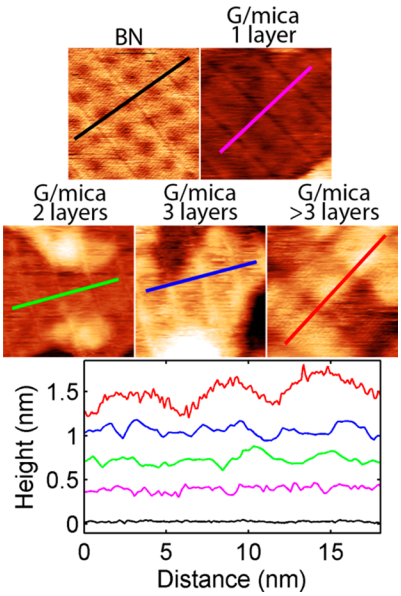

Figure 2. Comparison of the variation of heights across the lamellar rows for TTC adsorbed on different substrates (extracted from images in Figure 1). For TTC on G/BN and G/mica with 1−3 water layers, the corrugation amplitude is below 0.1 nm. A larger and more regular corrugation is found for >3 layers.

very low (<0.03 nm). On G/mica with 1−3 trapped water layers the periodic structure is larger than, but still comparable to, the background roughness ∼0.05 nm. However, when adsorbed on regions where there are >3 trapped water layers, the height variation shows a clear periodicity with a peak-to-peak height of 0.20−0.25 nm; these changes indicate that the underlying graphene substrate is deformable in regions where there are multiple trapped water layers, and adopts a corrugated conformation.

As we show below, the curvature of the surface results in an overall reduction in the total energy by increasing the interaction energy between the alkane chain and graphene at the expense of bending energies of the alkane chain and graphene sheet. As discussed above, on a flat surface, the carbon atoms in the alkane chain cannot all sit above their preferred adsorption sites on the graphene. However, this preferred registry may be recovered, at least partially, through the introduction of curvature. Here, we use a simple analytical model, complemented by molecular dynamics simulations, to show that adsorbate-induced curvature accounts for our experimental observations. Note that an alternate tip-induced mechanism for deformation of graphene that, unlike the arrangement discussed above, is in the form of a freely suspended membrane results in apparent radii of curvature that are two orders of magnitude larger than the values observed here.[26]

The elements of the model are shown schematically in Figure 3a. The lowest energy adsorption site for each $-CH_2-$ group is in alignment with the center of a hexagon in the underlying graphene ($s = 0$ in the schematic in Figure 3a). At position s along the alkane chain a given group is displaced out of registry by Δl ($= s\delta a/a$ to first order in δa). However, if we introduce

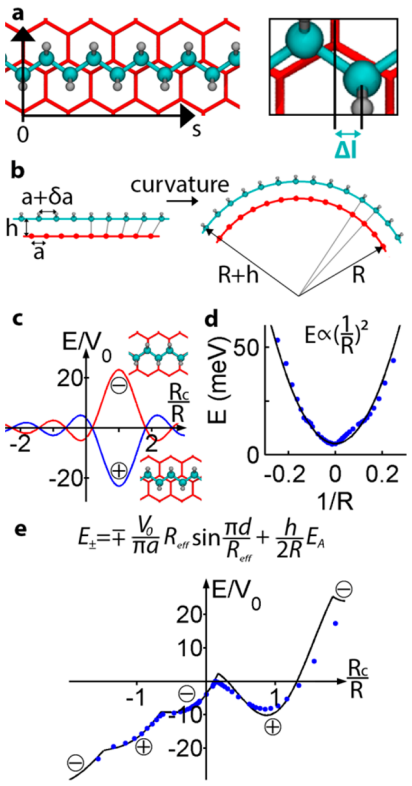

Figure 3. (a) Schematic of *n*-alkane adsorbed on G. The $-CH_2-$ group at $s = 0$ is positioned at the preferred adsorption site. Due to the mismatch in separation of carbon atoms in the chain and the graphene, the $-CH_2-$ groups along s are offset relative to their preferred adsorption site by an amount Δl ($\approx (s/a)\delta a$). (b) Schematic side view of the adsorption; in the flat configuration, the difference in periods leads to a variation in local registry. The variation of registry can be modified if the TTC/G surface is curved, and completely eliminated if the ratios of the arc lengths (periods) is equal to the ratio of radii of curvature, that is, $(a + \delta a)/a = (R + h)/R$, or $R = R_c = ha/\delta a$. (c) In-phase (blue) and out-of-phase (red) curvature dependent moiré variation of adsorption energy with respect to a surface with a radius of curvature R. (d) Bending energy of the adsorbed TTC versus inverse radius of curvature. (e) Adsorption energy of TTC on graphene (solid line) and numerical calculations (blue dots) for a curved graphene surface, indicating that the curvature-related moiré effect successfully accounts for the calculated behavior.

curvature, the relative displacement may be reduced (see Figure 3b) due to the difference in radius of curvature of the graphene, R, and the adsorbed molecule, $R + h$, where h is the separation of the alkane and graphene. Indeed, the preferred registry can be completely restored if $(a + \delta a)/a = (R + h)/R$ (Figure 3b). This is satisfied at a critical radius of curvature, $R_c = ah/\delta a = hR_m/a$, where R_m is a moiré length ($= a^2/\delta a$) associated with the mismatch between the alkane and graphene repeat lengths.

To estimate the energy gain arising from the introduction of curvature we write the adsorption energy for a pair of carbon atoms in the alkane chain as $V(s) = -V_0\cos(2\pi\Delta l(s)/a)$. On flat graphene $\Delta l(s) = (s/a)\delta a$, but for a constant radius of curvature, R, this is modified to $\Delta l(s) = (s/a)\delta a - hs/R$. We may generalize to a surface with spatially varying radius of curvature, $R(s)$, which gives $\Delta l(s) = (s/a)\delta a - h\theta(s)$, where $\theta(s)$ is given by $\int_0^s ds'/R(s')$. The curvature-dependent adsorption energy is then given by a sum over all carbon pairs, which we replace by a line integral

dx.doi.org/10.1021/nl503308c | Nano Lett. XXXX, XXX, XXX−XXX

$$E_{\pm} = \mp\frac{V_o}{a}\int_{-d/2}^{d/2}\cos 2\pi\left(\frac{\delta a}{a^2}s - \frac{h}{a}\theta(s)\right)\mathrm{d}s$$

Here, d is the molecular length ($d \approx Na$, where N is the number of carbon pairs in the alkane chain) and the $\pm$ solutions correspond to positioning the center of the alkane in either an energy minimum (+), or maximum (−); see schematic in Figure 3c.

There are several other curvature-dependent contributions to the total energy. First we include the expected background variation of the total adsorption energy for a curved surface; an atom at height h above a surface experiences a curvature-dependent contribution to the energy given by $E_A(R) = -(1 - h/2R)E_A$ arising from an increase in atom−surface separation for positive curvature (E_A is the total adsorption energy and the expression is valid to first order in (h/R); see Supporting Information for further discussion and a derivation). The energy cost of bending the alkane is given by

$$E_B = \frac{\kappa_B}{2}\int_{-d/2}^{d/2}\frac{1}{R^2}\mathrm{d}s$$

where we treat the molecule as an elastic rod with bending coefficient κ_B. For an isotropic graphene monolayer, the bending energy is given by

$$E = \frac{\kappa}{2}\int\frac{1}{R^2}\mathrm{d}A$$

where κ is the bending coefficient, which has been estimated[27,28] to be $\kappa = 0.19$ nN nm. In the equation below, we include the factor $a\sqrt{3}$, the separation of molecules along the lamellar rows, in the term for the graphene bending energy, because we consider the energy per molecule on a corrugated surface.

The total energy per molecule due to bending can thus be written, noting that $R(s)^{-1} = \mathrm{d}\theta/\mathrm{d}s$

$$E = -\int_{-d/2}^{d/2}\left[\frac{V_o}{a}\cos 2\pi\left(\frac{\delta a}{a^2}s - \frac{h}{a}\theta(s)\right) - E_A\frac{h}{2}\frac{\mathrm{d}\theta}{\mathrm{d}s} - \frac{\kappa_B}{2}\left(\frac{\mathrm{d}\theta}{\mathrm{d}s}\right)^2 - \frac{\kappa a\sqrt{3}}{2}\left(\frac{\mathrm{d}\theta}{\mathrm{d}s}\right)^2\right]\mathrm{d}s \quad (1)$$

The contribution from the curvature-dependent moiré effect may be understood by integrating the first term for a surface with constant cylindrical curvature R. This gives

$$E_{\pm} = \mp(V_0/\pi a)R_{\mathrm{eff}}\sin(\pi d/R_{\mathrm{eff}})$$

where R_{eff} is a curvature-dependent moiré length, $R_{\mathrm{eff}}^{-1} = R_m^{-1}(1 - hR_m/aR)$. This contribution to the energy has the functional form of $\mathrm{sinc}(R_{\mathrm{eff}}^{-1})$ and is plotted in Figure 3c; at $R = R_c$, there is an energy minimum with a value $-NV_0$ because all carbon pairs are in their preferred positions for this curvature (note that this corresponds to an infinite value for the curvature-dependent moiré length, R_{eff}, consistent with the above formula because $R_c = hR_m/a$).

For inverse curvatures close to this minimum, $R^{-1} = R_c^{-1} + \delta(R^{-1})$ the dependence on energy may be expanded as

$$E = -NV_o + (\kappa_m d/2)\delta(R^{-1})^2$$

where we introduce the moiré-induced bending stiffness, $\kappa_m = \pi^2 dh^2 NV_o/3a^2$. The energy in Figure 3c oscillates and adopts negative values for curvatures where more of the carbon pairs in the chain are in unfavorable registry with the graphene sheet; note that in these regions, the E_- solutions are lower in energy.

We have used molecular dynamics simulations to investigate whether this analytical model correctly describes the minimum energy configuration of an alkane chain on a curved graphene surface. The Large-scale Atomic/Molecular Massively Parallel Simulator (LAMMPS) classical molecular dynamics code[29] was used in conjunction with the Adaptive Intermolecular Reactive Empirical Bond Order (AIREBO) potential which has been developed to describe hydrocarbon systems.[30] The AIREBO potential is an improved version of Brenner's well-known second generation Reactive Empirical Bond Order Potential,[31] which includes a Lennard-Jones term to model van der Waals interactions and a torsional term to describe torsions of σ-bonds (computational details are included in the Supporting Information) .

Using this approach, we optimize a TTC molecule adsorbed on a frozen cylindrical graphene surface (a zigzag nanotube, but with an artificially large radius of curvature). We extract the dependence on curvature, R^{-1}, of the adsorption energy and the bending energy of the adsorbed alkane. These calculations confirm that the alkane is adsorbed with the zigzag chain locally parallel to the graphene at a height, $h = 0.38$ nm, which is near-independent of curvature. The calculated values for $E_A = -3.33$ eV, and the barrier energy $V_0 = 6$ meV, are in excellent agreement with previous calculations[32−34] and may be used to estimate the moiré-induced bending stiffness, $\kappa_m = 1.0$ nNnm^2. In addition, we extract from our simulations the intrinsic bending energy of the alkane, E_B (see Figure 3d), which is expected to have the form $E_B = \kappa_B d/2R^2$; we find the expected parabolic dependence on R^{-1} and determine the alkane bending coefficient to be $\kappa_B = 0.04$ nN nm^2.

Figure 3e shows a comparison of the theoretical adsorption energy, with the numerically calculated values (blue points). Despite the simplicity of the model, the principal physical results are captured correctly. In particular, we observe an energy minimum for $R \approx R_c$ corresponding to the matching condition discussed above, combined with a background linear slope. The cusp-like behavior, at the curvatures where the red and blue curves in Figure 3c intersect, is due to the lowest energy configuration, which always results from numerical optimization, undergoing a transition from an in-phase (+) to an out-of-phase (−) solution. This comparison confirms that the simple, analytic form (eq 1) accounts for the calculated variation of adsorption energy and that no other deformation processes, such as bond angle distortion and other elastic effects, play a significant role.

Our experimental configuration differs from this simple scenario since the average curvature over the surface is zero, that is, it is macroscopically flat with regions of positive and negative curvature. To determine the stability of a surface against curvature, we consider the energy change arising from a variation in $\theta(s)$ which is periodic with period d, that is, $\theta(s) = \theta_0\sin 2\pi s/d$. For small amplitude variations, this gives a quadratic energy dependence with a minimum at $\theta_0 \neq 0$ confirming that spontaneous curvature due to molecular adsorption is expected. Neglecting the contributions from the bending energy terms proportional to κ and κ_B, results in a predicted peak-to-peak height variation ($= \theta_o d/\pi$), $A = adf(\gamma)/4\pi^2 h$, where $f(\gamma) = \gamma(4 - \gamma^2)/(1 - \gamma^2)$ and the ratio $\gamma = d/R_m$. Inclusion of the intrinsic bending energies of the graphene and the molecule leads to a reduction in amplitude, A, by a factor $\beta = (1 + \alpha(\kappa_B + \kappa a\sqrt{3})/\kappa_m)^{-1}$ (where $\alpha = \pi^3\gamma(4 - \gamma^2)/$

dx.doi.org/10.1021/nl503308c | Nano Lett. XXXX, XXX, XXX−XXX

$[12\sin(\pi\gamma)]$; all derivations are included in Supporting Information), which can vary between 0 and 1.

Experimentally, we find $A = 0.22 \pm 0.02$ nm, which using the values of κ_m, κ_B, κ, and h discussed above, implies $\gamma = 0.66 \pm 0.04$ and $\beta = 0.55$. This in turn implies that $R_m \approx 3d/2$ and, recalling that $R_m = a^2/\delta a$, gives $\delta a \sim 2a/3N \sim 0.03a \approx 7$ pm. This corresponds to a spacing of carbon pairs in the alkane of $a_{alk} = 0.253$ nm. This value is slightly larger than assumed previously[15−17] (0.251 nm) but is close to published values for carbon atoms in propane, 0.2536 nm.[35] Note that these differences, which are in the picometer scale, are significant since the amplitude, A, is proportional to the difference between periodicities between graphite and the alkane. This agreement supports our interpretation of adsorbate-induced curvature of graphene.

For graphene adhering to a solid substrate surface, the bending coefficient κ should be replaced by that of the underlying substrate, which would be orders of magnitude higher. Consequently, $\beta \rightarrow 0$ and no spontaneous curvature would be expected; this corresponds to the case of hBN. Interestingly, the adsorbate-induced stiffness, κ_m, is much larger than the combined intrinsic stiffness per molecule of the graphene and alkane, $\kappa_m \gg (\kappa_B + \kappa a\sqrt{3})$. Thus, the energy cost of displacing atoms in the alkane chain from their preferred adsorption sites is much greater than the intrinsic energy cost of bending either the graphene or the alkane.

Accordingly the alkane not only introduces corrugations but also an increased stiffness perpendicular to the lamellar rows, so that fluctuations around the corrugated configuration are suppressed relative to fluctuations along the rows. It has previously been shown[28] that the fluctuation amplitude is inversely proportional to $\kappa^{1/2}$; in our case, the stiffness is highly anisotropic and we attribute the observation of anisotropic height fluctuations in Figure 1f to this effect. We also note that recent measurements have shown that the bending stiffness of bilayer graphene is significantly greater than that of monolayer.[36] It is possible that this is also related to the relative displacement of carbon atoms in one layer from their preferred adsorption site on a neighboring layer.

Overall, our work shows that transferred graphene can undergo elastic deformation that is induced by the adsorption of supramolecular structures. This effect is induced through the adsorption of alkanes, but it is likely that other organic molecules will also induce deformations when adsorbed on graphene. This is relevant both to free surfaces of graphene and also to buried interfaces between graphene and, for example, polymers in composite materials and fabricated structures. This finding is relevant to applications in microfluidics, electronics, composite materials, and nanomechanical systems, both in terms of gaining improved understanding of device operation and also for new modalities, for example, related to control of mechanical properties. Our work also provides an example of supramolecular organization on a soft support. The property of mechanical deformability of such an "active" substrate in response to adsorbates is reminiscent of interfaces encountered in biological systems, and our work motivates further studies of adsorption on soft supports, both those derived from graphene membranes and also those interfaces formed between other responsive materials.

■ ASSOCIATED CONTENT

Supporting Information

STM data acquisition and image processing, sample preparation, graphene growth and characterization, additional STM images, analysis of adsorption energy of alkanes on curved graphene, numerical and computational details, and error analysis. This material is available free of charge via the Internet at http://pubs.acs.org.

■ AUTHOR INFORMATION

Corresponding Author

*E-mail: peter.beton@nottingham.ac.uk.

Notes

The authors declare no competing financial interest.

■ ACKNOWLEDGMENTS

We acknowledge financial support from the U.K. Engineering and Physical Science Research Council (EPSRC) under grant number EP/K01773X/1. We thank the University of Nottingham High Performance Computing (HPC) facility for provision of computational time. E.B. gratefully acknowledges receipt of an ERC Consolidator Grant.

■ REFERENCES

(1) Wehling, T. O.; Novoselov, K. S.; Morozov, S. V.; Vdovin, E. E.; Katsnelson, M. I.; Geim, A. K.; Lichtenstein, A. I. *Nano Lett.* **2008**, *8*, 173−177.
(2) Schedin, F.; Geim, A. K.; Morozov, S. V.; Hill, E. W.; Blake, P.; Katsnelson, M. I.; Novoselov, K. S. *Nat. Mater.* **2007**, *6*, 652−655.
(3) Chen, W.; Chen, S.; Qi, D. C.; Gao, X. Y.; Wee, A. T. S. *J. Am. Chem. Soc.* **2007**, *129*, 10418−10422.
(4) Wang, Q. H.; Hersam, M. C. *Nat. Chem.* **2009**, *1*, 206−211.
(5) Mao, J.; Zhang, H.; Jiang, Y.; Pan, Y.; Gao, M.; Xiao, W.; Gao, H.-J. *J. Am. Chem. Soc.* **2009**, *131*, 14136−14137.
(6) Pollard, A. J.; Perkins, E. W.; Smith, N. A.; Saywell, A.; Goretzki, G.; Phillips, A. G.; Argent, S. P.; Sachdev, H.; Müller, F.; Hüfner, S.; Gsell, S.; Fischer, M.; Schreck, M.; Osterwalder, J.; Greber, T.; Berner, S.; Champness, N. R.; Beton, P. H. *Angew. Chem., Int. Ed. Engl.* **2010**, *49*, 1794−1799.
(7) Sun, X.; Zhang, J.; Wang, X.; Zhang, C.; Hu, P.; Mu, Y.; Wan, X.; Guo, Z.; Lei, S. *Chem. Commun.* **2013**, *49*, 10317−10319.
(8) Järvinen, P.; Hämäläinen, S. K.; Banerjee, K.; Häkkinen, P.; Ijäs, M.; Harju, A.; Liljeroth, P. *Nano Lett.* **2013**, *13*, 3199−3204.
(9) Li, B.; Tahara, K.; Adisoejoso, J.; Vanderlinden, W.; Mali, K. S.; De Gendt, S.; Tobe, Y.; De Feyter, S. *ACS Nano* **2013**, *7*, 10764−10772.
(10) Li, J.; Wieghold, S.; Öner, M. A.; Simon, P.; Hauf, M. V.; Margapoti, E.; Garrido, J. A.; Esch, F.; Palma, C.; Barth, J. V. *Nano Lett.* **2014**, *14*, 4486−4492.
(11) Meyer, J. C.; Geim, A. K.; Katsnelson, M. I.; Novoselov, K. S.; Booth, T. J.; Roth, S. *Nature* **2007**, *446*, 60−63.
(12) Li, X.; Cai, W.; An, J.; Kim, S.; Nah, J.; Yang, D.; Piner, R.; Velamakanni, A.; Jung, I.; Tutuc, E.; Banerjee, S. K.; Colombo, L.; Ruoff, R. S. *Science* **2009**, *324*, 1312−1314.
(13) Dean, C. R.; Young, A. F.; Meric, I.; Lee, C.; Wang, L.; Sorgenfrei, S.; Watanabe, K.; Taniguchi, T.; Kim, P.; Shepard, K. L.; Hone, J. *Nat. Nanotechnol.* **2010**, *5*, 722−726.
(14) Lui, C. H.; Liu, L.; Mak, K. F.; Flynn, G. W.; Heinz, T. F. *Nature* **2009**, *462*, 339−341.
(15) Rabe, J. P.; Buchholz, S. *Science* **1991**, *253*, 424−427.
(16) McGonigal, G. C.; Bernhardt, R. H.; Thomson, D. J. *Appl. Phys. Lett.* **1990**, *57*, 28.
(17) Cyr, D. M.; Venkataraman, B.; Flynn, G. W. *Chem. Mater.* **1996**, *4756*, 1600−1615.

(18) Yankowitz, M.; Xue, J.; Cormode, D.; Sanchez-Yamagishi, J. D.; Watanabe, K.; Taniguchi, T.; Jarillo-Herrero, P.; Jacquod, P.; LeRoy, B. J. *Nat. Phys.* **2012**, *8*, 382−386.
(19) Xue, J.; Sanchez-Yamagishi, J.; Bulmash, D.; Jacquod, P.; Deshpande, A.; Watanabe, K.; Taniguchi, T.; Jarillo-Herrero, P.; LeRoy, B. J. *Nat. Mater.* **2011**, *10*, 282−285.
(20) Decker, R.; Wang, Y.; Brar, V. W.; Regan, W.; Tsai, H.; Wu, Q.; Gannett, W.; Zettl, A.; Crommie, M. F. *Nano Lett.* **2011**, *11*, 2291−2295.
(21) Xu, K.; Cao, P.; Heath, J. R. *Science* **2010**, *329*, 1188−1191.
(22) He, K. T.; Wood, J. D.; Doidge, G. P.; Pop, E.; Lyding, J. W. *Nano Lett.* **2012**, *12*, 2665−2672.
(23) Shim, J.; Lui, C. H.; Ko, T. Y.; Yu, Y.-J.; Kim, P.; Heinz, T. F.; Ryu, S. *Nano Lett.* **2012**, *12*, 648−654.
(24) Kim, J.-S.; Choi, J. S.; Lee, M. J.; Park, B. H.; Bukhvalov, D.; Son, Y.-W.; Yoon, D.; Cheong, H.; Yun, J.-N.; Jung, Y.; Park, J. Y.; Salmeron, M. *Sci. Rep.* **2013**, *3*, 2309.
(25) Severin, N.; Lange, P.; Sokolov, I. M.; Rabe, J. P. *Nano Lett.* **2012**, *12*, 774−779.
(26) Klimov, N. N.; Jung, S.; Zhu, S.; Li, T.; Wright, C. A.; Solares, S. D.; Newell, D. B.; Zhitenev, N. B.; Stroscio, J. A. *Science* **2012**, *336*, 1557−1561.
(27) Lu, Q.; Arroyo, M.; Huang, R. *J. Phys. D: Appl. Phys.* **2009**, *42*, 102002.
(28) Fasolino, A.; Los, J. H.; Katsnelson, M. I. *Nat. Mater.* **2007**, *6*, 858−861.
(29) Plimpton, S. *J. Comput. Phys.* **1995**, *117*, 1−19.
(30) Stuart, S. J.; Tutein, A. B.; Harrison, J. A. *J. Chem. Phys.* **2000**, *112*, 6472.
(31) Brenner, D. W.; Shenderova, O. A.; Harrison, J. A.; Stuart, S. J.; Ni, B.; Sinnott, S. B. *J. Phys.: Condens. Matter* **2002**, *14*, 783−802.
(32) Kamiya, K.; Okada, S. *Jpn. J. Appl. Phys.* **2013**, *52*, 06GD10.
(33) Yang, T.; Berber, S.; Liu, J.-F.; Miller, G. P.; Tománek, D. *J. Chem. Phys.* **2008**, *128*, 124709.
(34) Hentschke, R.; Schürmann, B. L.; Rabe, J. P. *J. Chem. Phys.* **1992**, *96*, 6213.
(35) NIST Database. http://cccbdb.nist.gov/expgeom2.asp?casno=74986 (accessed Oct 2014).
(36) Lindahl, N.; Midtvedt, D.; Svensson, J.; Nerushev, O. A.; Lindvall, N.; Isacsson, A.; Campbell, E. E. B. *Nano Lett.* **2012**, *12*, 3526−3531.